© 2014. Published by The Company of Biologists Ltd | Journal of Cell Science (2014) 127, 4396–4408 doi:10.1242/jcs.148098

RESEARCH ARTICLE

CFTR interacts with ZO-1 to regulate tight junction assembly and epithelial differentiation through the ZONAB pathway

Ye Chun Ruan[1,2], Yan Wang[2], Nicolas Da Silva[1], Bongki Kim[1], Rui Ying Diao[2], Eric Hill[1], Dennis Brown[1], Hsiao Chang Chan[2] and Sylvie Breton[1,*]

ABSTRACT

Mutations in CFTR lead to dysfunction of tubular organs, which is currently attributed to impairment of its conductive properties. We now show that CFTR regulates tight junction assembly and epithelial cell differentiation through modulation of the ZO-1–ZONAB pathway. CFTR colocalizes with ZO-1 at the tight junctions of trachea and epididymis, and is expressed before ZO-1 in Wolffian ducts. CFTR interacts with ZO-1 through the CTFR PDZ-binding domain. In a three-dimensional (3D) epithelial cell culture model, CFTR regulates tight junction assembly and is required for tubulogenesis. CFTR inhibition or knockdown reduces ZO-1 expression and induces the translocation of the transcription factor ZONAB (also known as YBX3) from tight junctions to the nucleus, followed by upregulation of the transcription of *CCND1* and downregulation of *ErbB2* transcription. The epididymal tubules of $cftr^{-/-}$ and $cftr^{\Delta F508}$ mice have reduced ZO-1 levels, increased ZONAB nuclear expression, and decreased epithelial cell differentiation, illustrated by the reduced expression of apical AQP9 and V-ATPase. This study provides a new paradigm for the etiology of diseases associated with CFTR mutations, including cystic fibrosis.

KEY WORDS: CFTR, ZO-1, ZONAB, Embryonic development, Epithelial remodeling, Male fertility, Morphogenesis, Proliferation

INTRODUCTION

Mutations of the cystic fibrosis transmembrane conductance regulator (*CFTR*) gene lead to cystic fibrosis (CF), the most common autosomal recessive disease in Caucasian populations. CF affects the function of several organs, in particular the trachea, lung, pancreas and several tissues of the reproductive system (Chan et al., 2009; Guggino and Stanton, 2006; O'Sullivan and Freedman, 2009; Quinton, 1999; Rowe et al., 2005). Almost all male CF patients are diagnosed with congenital bilateral absence of the vas deferens (CBAVD) and concurrent absence or atrophy of a large portion of the epididymis (Anguiano et al., 1992; Cuppens and Cassiman, 2004; Oates and Amos, 1994; Patrizio and Zielenski, 1996; Yu et al., 2012). These organs are located downstream of the testis; they are required for sperm maturation, storage and transport, and are thus essential for the establishment of male fertility (Chen et al., 2012b; Cornwall, 2009; Robaire et al., 2006; Shum et al., 2011). In addition, men carrying silent mutations of CFTR that do not cause CF have reduced fertility while being otherwise healthy, indicating that the male reproductive organs are among the most affected by these mutations (Chan et al., 2009; Cuppens and Cassiman, 2004; Schulz et al., 2006; van der Ven et al., 1996).

CFTR is a cAMP-activated anion channel located in the apical membrane of secretory epithelia. Defects in chloride, bicarbonate and water secretion, leading to increased viscosity of the luminal compartment, were proposed as the primary cause of CF and CBAVD (Bomberger et al., 2011; Guggino and Stanton, 2006; Joseph et al., 2009). More recently, CFTR-knockout pigs further showed CFTR-mediated fluid absorption in the alveolar epithelium, indicating the role of mutant CFTR in respiratory distress syndrome and pulmonary edema (Li et al., 2012). In addition, acidification of the airway surface liquid due to defective CFTR-dependent bicarbonate secretion impairs bacterial killing in these animals (Pezzulo et al., 2012). Current treatments for CF include the use of antibiotics, anti-inflammatory and mucolytic agents, pancreatic enzyme diet supplementation and chest physiotherapy (Galietta, 2013). However, these treatments target the consequences of CF rather than the actual cause of the disease (Ramsey et al., 2012). Novel therapeutic strategies are now aimed at correcting the anion channel function of CFTR by improving its gating activity or its plasma membrane insertion, which are both impaired by the mutations (Galietta, 2013; Rowe and Verkman, 2013). As highlighted in a recent National Heart, Lung, and Blood Institute workshop report "emerging evidence suggests that CF lung disease begins in infancy and is initially 'silent' without overt signs or symptoms" (Ramsey et al., 2012). However, a reduced tracheal caliber and airway cross-sectional area have been observed even in newborn CFTR-knockout pigs and young CF patients (Meyerholz et al., 2010). CFTR is highly expressed in the epithelial cells lining the epididymis, vas deferens and respiratory tract, and it is detected in the human fetus at early developmental stages (Gaillard et al., 1994; Hihnala et al., 2006; Pietrement et al., 2008; Ruan et al., 2012; Ruz et al., 2004; Tizzano et al., 1993). Taken together, these data indicate that CFTR might play an as-yet-undefined role, in addition to its ion channel function, during development.

During embryonic development and tissue repair, epithelial cells switch from proliferation to differentiation states, a process that depends on cell density and is modulated by ZO-1 nucleic acid binding protein (ZONAB, also known as YBX3), a Y box transcription factor that controls the expression of genes involved in cell growth and differentiation (Balda and Matter, 2000; Lima

[1]Center for Systems Biology, Program in Membrane Biology, Nephrology Division, Massachusetts General Hospital, Harvard Medical School, Boston, MA 02114, USA. [2]Epithelial Cell Biology Research Center, School of Biomedical Sciences, Faculty of Medicine, The Chinese University of Hong Kong, Hong Kong, China.

*Author for correspondence (Breton.sylvie@mgh.harvard.edu)

Received 13 December 2013; Accepted 17 July 2014

Journal of Cell Science

et al., 2010; Sourisseau et al., 2006). The tight-junction-associated protein ZO-1 inhibits cell proliferation and promotes differentiation by sequestration of ZONAB outside of the nucleus at tight junctions (Balda and Matter, 2009). Deletion of ZO-1 in mice leads to embryonic death at around mid-gestation (Katsuno et al., 2008). The C-terminus of CFTR contains a PDZ-binding domain (Guggino and Stanton, 2006), and we explored the possibility that CFTR might interact with ZO-1 and participate in the modulation of the ZO-1–ZONAB pathway.

Given the severe developmental defects in the male reproductive organs caused by CFTR mutations, we used the epididymis as a model system to examine possible roles for CFTR in tight junction dynamics, during both prenatal and postnatal development. Here, we show that a significant portion of CFTR is located at tight junctions, where it interacts with ZO-1 through its PDZ-binding domain, and modulates the expression of proliferation and differentiation genes that are under the control of the ZO-1–ZONAB pathway. In addition, two independent markers of epithelial cell differentiation, AQP9 in principal cells and V-ATPase in clear cells, were significantly reduced in *cftr*$^{-/-}$ mice. Our study, therefore, reveals a novel connection between CFTR and epithelial morphogenesis and differentiation.

RESULTS

CFTR is located in epididymal tight junctions and interacts with ZO-1 through its PDZ-binding domain

The epididymis was used as a model system to examine the potential participation of CFTR in tight junction dynamics. In addition to its previously described expression in the apical membrane of principal cells (Pietrement et al., 2008; Ruan et al., 2012; Ruz et al., 2004), CFTR was also detected in the apical intercellular junctions of the epithelium (Fig. 1A). Pre-incubation of the antibody with the immunizing peptide abolished the labeling for CFTR (Fig. 1Ac), confirming antibody specificity. Confocal laser scanning microscopy analysis revealed the colocalization of CFTR with ZO-1 (Fig. 1B), showing that CFTR is located at tight junctions. CFTR is also located in the apical membrane (arrowheads) but is absent from the lateral membrane (arrows). In addition, CFTR colocalized with ZO-1 at tight junctions in a mouse epididymal cell line, DC2 (Fig. 1C). CFTR co-immunoprecipitated with ZO-1 from mouse epididymis protein extracts using the anti-ZO-1 antibody (Fig. 1D), indicating that CFTR forms a protein complex with ZO-1. CFTR also co-immunoprecipitated with ZO-1 in DC2 cells (Fig. 1E) and, reciprocally, ZO-1 co-immunoprecipitated with CFTR using the anti-CFTR antibody in these cells (Fig. 1F).

The C-terminus of CFTR contains a PDZ-binding motif (DTRL) that mediates its interaction with several proteins (Guggino and Stanton, 2006). Therefore, we tested the participation of this motif in the CFTR–ZO-1 interaction. Chinese hamster ovary (CHO) cells were transfected with full-length human CFTR (hCFTRwt) or a mutated human CFTR construct in which the PDZ-binding coding sequence was deleted (hCFTRΔpdzb). Western blot analysis showed that both hCFTRwt and hCFTRΔpdzb were expressed at 48 hours after transfection; the lower level of hCFTRΔpdzb expression indicates higher degradation and/or lower synthesis rate of this mutated protein (Fig. 1G, left panel). A low level of endogenous CFTR protein was also detected in these cells. The interaction of both wild-type and mutated CFTR with ZO-1, which is expressed endogenously in CHO cells, was then analyzed by co-immunoprecipitation. The respective protein levels were first adjusted to obtain similar amounts of hCFTRΔpdzb and hCFTRwt in the immunoprecipitation input (Fig. 1G, middle panel). Although the anti-ZO-1 antibody co-immunoprecipitated CFTR from both hCFTRwt- and hCFTRΔpdzb-transfected cells (Fig. 1G, right panel), a much weaker signal was obtained in hCFTRΔpdzb-transfected cells compared with the hCFTRwt cells, despite the higher amount of ZO-1 in the concentrated material used to perform the co-immunoprecipitation assay when using hCFTRΔpdzb-transfected cells. These results show the participation of the CFTR PDZ-binding motif in the CFTR–ZO-1 interaction.

CFTR regulates tight junction assembly and controls tubulogenesis in cultured epididymal epithelial cells

We then examined the potential participation of CFTR in tight junction dynamics in DC2 cells. As a read-out of tight junction assembly during cell culture growth, transepithelial electrical resistance (TER) was measured every day for 5 days after seeding. Cells were grown under control conditions or in different concentrations (0.1, 1, 10 and 50 μM) of the CFTR inhibitor CFTRinh172 (Ma et al., 2002). Maximal TER was reached under control conditions on day 3 and remained high up to day 5 (Fig. 2A). CFTRinh172 significantly reduced TER from day 2 to day 5 in a dose-dependent manner. Tight junctions disassemble in the absence of extracellular Ca^{2+} and re-assemble following the addition of Ca^{2+} back into the cultures (Martinez-Palomo et al., 1980). Here, we applied this 'Ca^{2+} switch' model to test for the role of CFTR in the reassembly of tight junctions in DC2 cells. As shown in Fig. 2B, whereas TER recovered gradually 1, 2 and 3 hours after Ca^{2+} re-addition under control conditions, CFTRinh172 (10 μM) induced a significantly lower TER recovery compared with that of control. Immunofluorescent labeling for ZO-1 24 hours after Ca^{2+} re-addition showed a uniformly linear ZO-1 labeling pattern in control cells, indicating intact tight junctions (Fig. 2C, left). By contrast, CFTRinh172 (10 μM) induced a mostly fragmented and cytosolic ZO-1 labeling pattern (Fig. 2C, right), indicating impairment in tight junction reassembly after CFTR inhibition. The contribution of CFTR to tight junction assembly was further confirmed using small interfering (si)RNA-mediated CFTR knockdown. DC2 cells transfected with CFTR-specific siRNA (siRNAcftr) expressed markedly lower amounts of CFTR compared with cells transfected with siRNA targeting a scrambled sequence (siRNAnc), demonstrating the effectiveness of knockdown (Fig. 2D). Cells treated with siRNAcftr had lower TER values compared with those of control cells treated with siRNAnc on day 2 and day 3 after transfection and seeding (Fig. 2E). A Ca^{2+} switch experiment, performed 72 hours after transfection, showed inhibition of TER recovery in cells treated with siRNAcftr compared with siRNAnc-treated control cells (Fig. 2F). More fragmented and cytosolic ZO-1 immunofluorescent labeling was observed 3 hours after Ca^{2+} re-addition in siRNAcftr-treated cells compared with siRNAnc-controls (Fig. 2G).

We next established an *in vitro* epithelial tubulogenesis model using DC2 cells cultured on Matrigel. Conventional brightfield microscopy showed that DC2 cells formed elongated structures when cultured under control conditions (Fig. 2H, Ctrl). By contrast, CFTRinh172 inhibited the formation of these tubule-like structures in a dose-dependent manner (Fig. 2H). Three-dimensional (3D) confocal microscopy reconstruction confirmed the formation of tubules that developed a luminal compartment in control cells treated with siRNAnc grown under

Journal of Cell Science (2014) 127, 4396–4408 doi:10.1242/jcs.148098

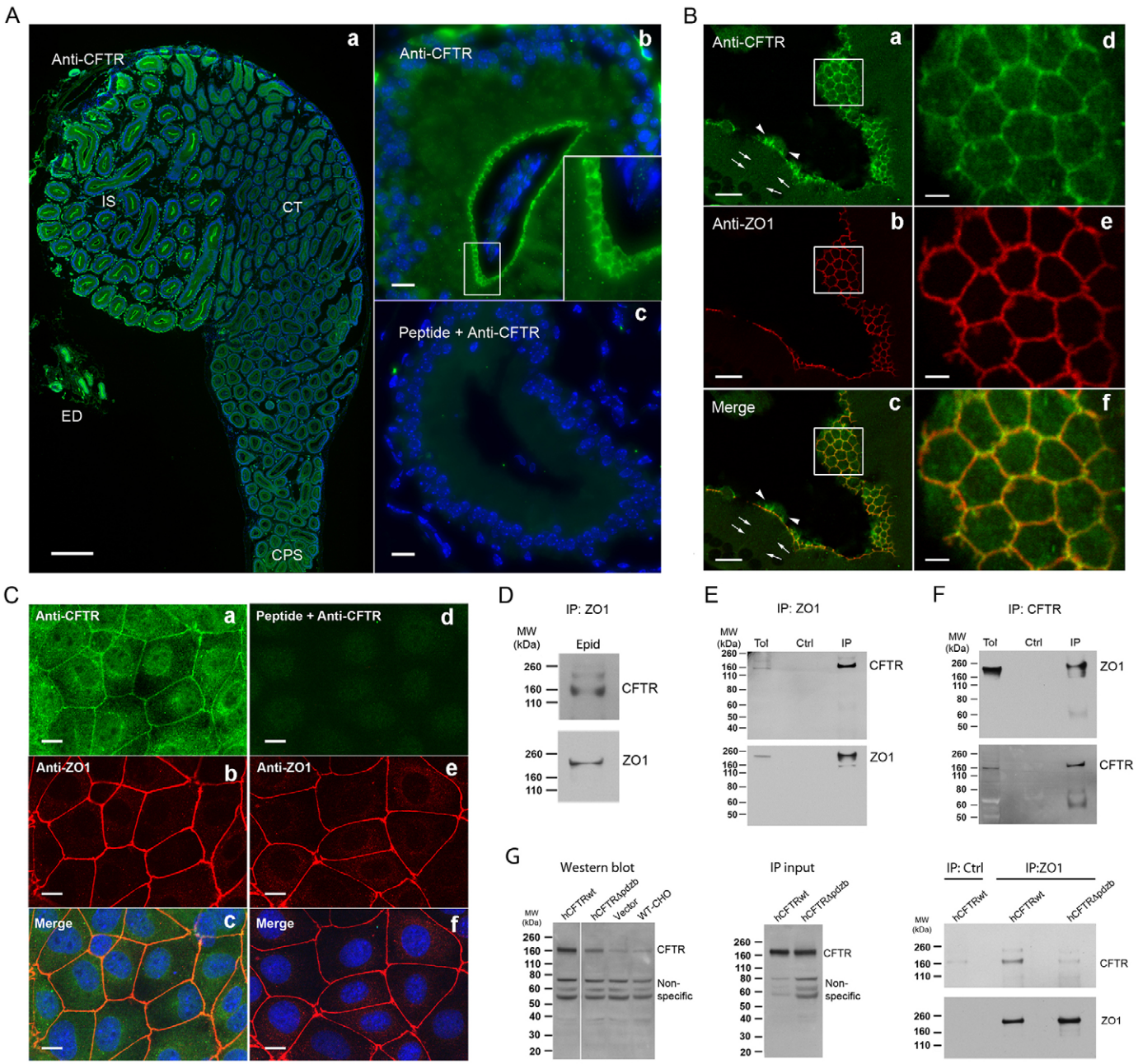

Fig. 1. CFTR is located at tight junctions and interacts with ZO-1 through its PDZ-binding domain. (Aa) Immunofluorescent labeling of CFTR in the proximal mouse epididymis. IS, initial segment; ED, efferent duct; CT, caput; CPS, corpus. (Ab) CFTR labeling (green) in apical epithelial cell–cell junctions in the initial segment. The inset shows a higher magnification view of the area outlined in white. (Ac) Pre-incubation of the CFTR antibody with the immunizing peptide prevents immunofluorescent labeling of CFTR. (Ba–c) Confocal laser scanning microscope images showing colocalization of CFTR (green) and ZO-1 (red) at tight junctions in the initial segment. Arrowheads, localization of CFTR in the apical membrane; arrows, absence of CFTR from the lateral membrane. (Bd–f) Higher magnification images of the regions delineated in the boxes in the left panels. Colocalization is indicated by the yellow/orange labeling in the merge panels (Bc,f). (Ca–c) Confocal laser scanning microscopy images showing colocalization of CFTR (green) and ZO-1 (red) at tight junctions of DC2 cells. Apical and intracellular CFTR labeling is also detected. (Cd–f) Pre-incubation of the CFTR antibody with the immunizing peptide prevents immunofluorescent labeling of CFTR. Nuclei are labeled in blue with DAPI (A) or Topro-3 (C). Scale bars: 300 μm (Aa); 10 μm (Ab,c, Ba–c); 2.5 μm (Bd–f); 5 μm (C).
(D) Immunoprecipitation (IP) of CFTR with ZO-1 in mouse epididymal (epid) protein extracts. (E) Immunoprecipitation of CFTR with ZO-1 in DC2 protein extracts. Ctrl, Protein-A-conjugated beads alone; Tot, total protein extracts. (F) Immunoprecipitation of ZO-1 with CFTR from DC2 protein extracts. (G) Left, western blot of CHO cells transfected with wild-type human CFTR (hCFTRwt) and human CFTR lacking the last four amino acids (DTRL) (hCFTRΔpdzb). WT-CHO, non-transfected cells; Vector, cells transfected with an empty vector. Non-specific lower-molecular-mass bands were also detected using this antibody. Middle, the protein amount used for co-immunoprecipitation assays (IP input) was adjusted to obtain similar levels of hCFTRwt and hCFTRΔpdzb. Right, co-immunoprecipitation of wild-type human CFTR (hCFTRwt) and mutant (hCFTRΔpdzb) with ZO-1. IP: Ctrl, beads alone.

Journal of Cell Science

Journal of Cell Science (2014) 127, 4396–4408 doi:10.1242/jcs.148098

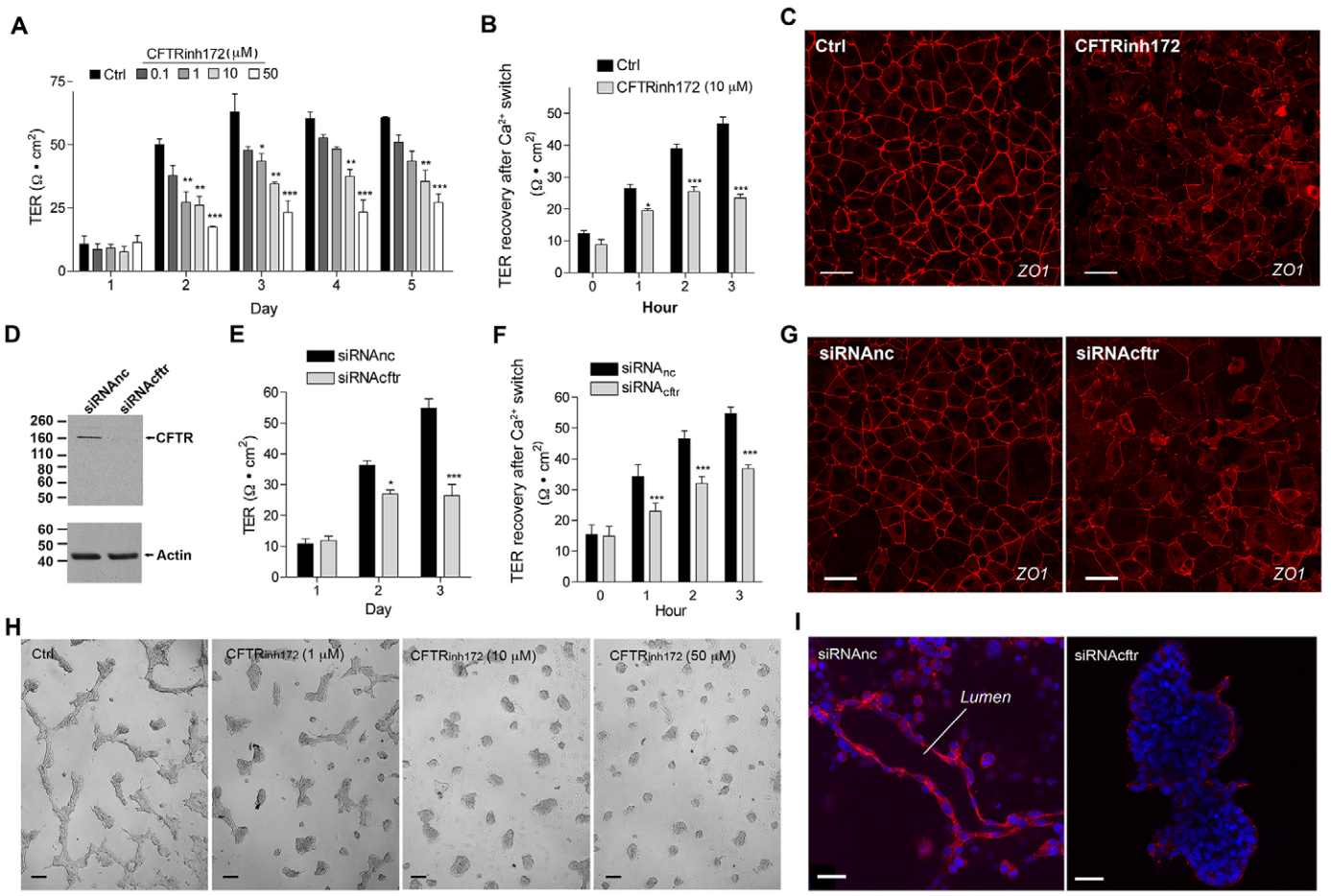

Fig. 2. CFTR deficiency impairs tight junction assembly and reassembly, and prevents tubulogenesis in DC2 cells. (A) TER in DC2 cultures treated with CFTRinh172 (0.1–50 μM) or DMSO (Ctrl) at 2, 3, 4 and 5 days after seeding (n=9). (B) DC2 confluent cultures were incubated in low-Ca^{2+} medium, and TER was measured every hour after switching the medium back to normal Ca^{2+} in the presence of CFTRinh172 (10 μM) or DMSO (Ctrl) (n=9). (C) ZO-1 labeling (red) in DC2 cultures 24 hours after the Ca^{2+} switch experiment in the presence of DMSO (Ctrl; left) or 10 μM CFTRinh172 (right). (D) Immunoblotting for CFTR in DC2 cells transfected for 3 days with CFTR-specific siRNAs (siRNAcftr) and cells transfected with non-silencing siRNAs as a negative control (siRNAnc) (upper panel). The same membrane was re-blotted for actin (lower panel). (E) TER in siRNAcftr- or siRNAnc-treated DC2 cells 1, 2 and 3 days after transfection and seeding (n=9). (F) TER values 1, 2 and 3 hours after the Ca^{2+} switch experiment in cells treated with siRNAcftr compared with those treated with siRNAnc (n=9). (G) ZO-1 labeling 3 hours after the Ca^{2+} switch experiment in DC2 cultures treated with siRNAcftr (right) or in control cells (siRNAnc; left). (H) Brightfield microscope images of DC2 cells cultured on a Matrigel layer under control conditions (Ctrl) or in the presence of CFTRinh172 (1, 10 and 50 μM). (I) Laser scanning confocal imaging for ZO-1 in control (siRNAnc-treated) DC2 cells (left) and siRNAcftr-treated cells (right). Nuclei are labeled in blue with Topro-3. 3D reconstruction animations can be seen in supplementary material Movies 1–4 (A,B,E,F) Data show the mean±s.e.m.; *P<0.05; **P<0.01; ***P<0.001 (by two-way ANOVA followed by Bonferroni's post hoc test). Scale bars: 20 μm (C,G,I); 50 μm (H).

control conditions (Fig. 2I, siRNAnc), whereas CFTR knockdown (Fig. 2I, siRNAcftr) inhibited the formation of these tubules and induced a disorganized cell growth with formation of cell masses lacking a lumen (supplementary material Movies 1–4).

CFTR regulates ZO-1 protein stability, and overexpression of ZO-1 prevents the effects of CFTR knockdown on tight junction assembly

Interestingly, inhibition of CFTR with CFTRinh172 (10 and 50 μM) induced a marked reduction of ZO-1 expression, and this effect occurred in a dose-dependent manner (Fig. 3A). Knockdown of CFTR also reduced ZO-1 expression (Fig. 3B). Real-time quantitative PCR showed that the mRNA level of ZO-1 was not significantly changed after CFTR knockdown (Fig. 3C), suggesting that the downregulation of ZO-1 occurred at the protein level, possibly by higher levels of degradation. In agreement with this notion, the downregulation of ZO-1 induced by CFTR knockdown was prevented in cells treated with the proteasome inhibitor MG-132 (10 μM) or the lysosome inhibitor leupeptin (10 μM) for 6 hours (Fig. 3D). These results indicate that CFTR regulates the stability of ZO-1.

We then determined whether the effects of CFTR knockdown on tight junction assembly could be overcome by preventing the downregulation of ZO-1 induced under these conditions. A DNA plasmid containing sequence encoding human ZO-1 (pZO-1) (Fanning and Anderson, 2002) or an empty vector plasmid (pVector) was applied to siRNAnc- and siRNAcftr-treated DC2 cells. As shown in Fig. 3E, 48 hours after co-transfection, transfection with the pZO-1 plasmid prevented the downregulation of ZO-1 induced after CFTR knockdown (compare lanes 3 and 4), whereas ZO-1 was still downregulated after CFTR knockdown in the pVector-treated cells (compare lanes 1 and 2). The Ca^{2+} switch assay was applied 48 hours after co-transfection to examine the remodeling

Journal of Cell Science (2014) 127, 4396–4408 doi:10.1242/jcs.148098

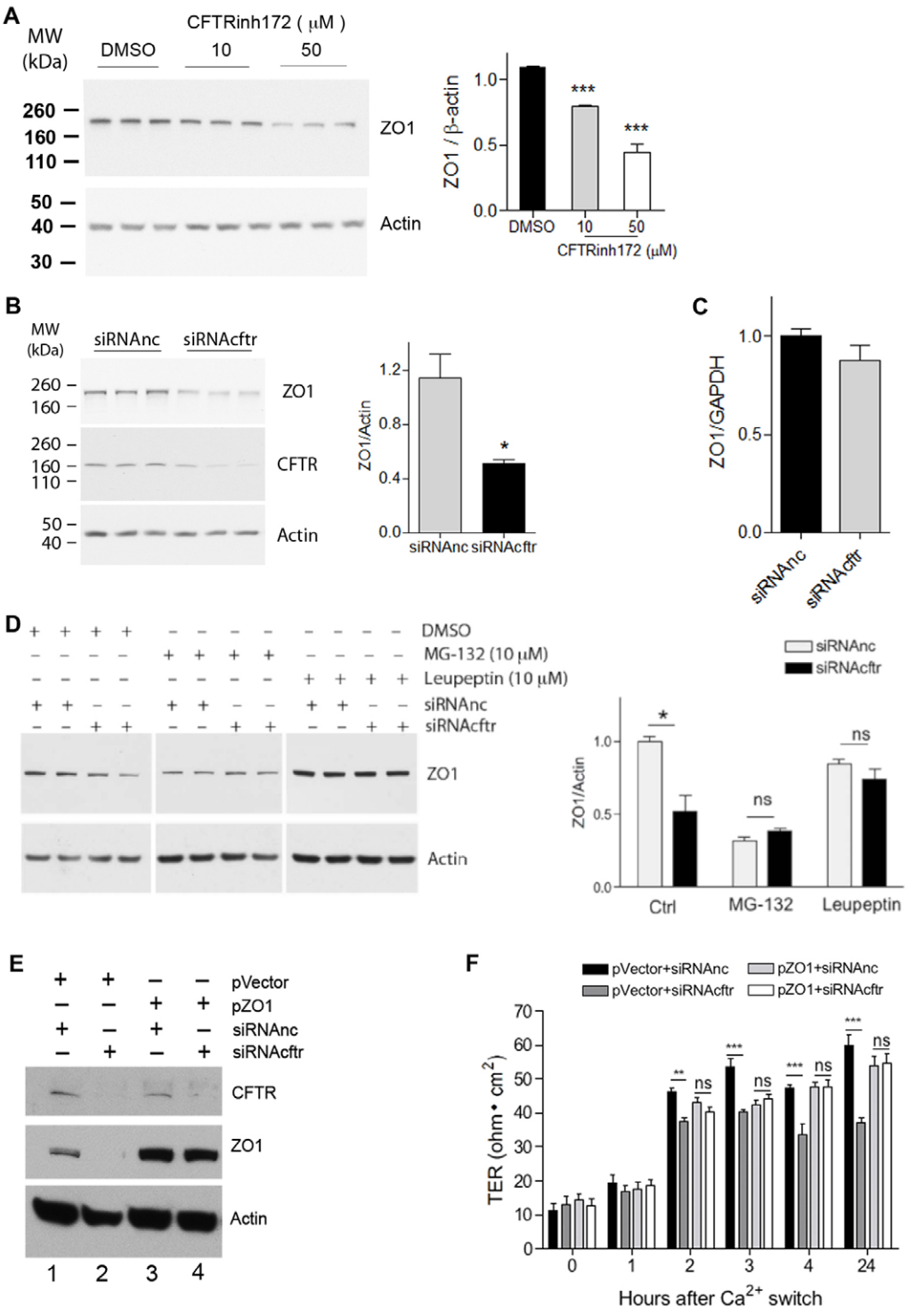

Fig. 3. CFTR regulates ZO-1 expression. (A) Left, immunoblotting for ZO-1 in DC2 cells treated for 3 days with CFTRinh172 (10 and 50 μM) and in control cells (DMSO). The same membrane was re-blotted for actin (lower panel). Right, quantification of ZO-1 expression normalized for actin in the presence of CFTRinh172 (10 and 50 μM) and in controls (DMSO). (B) Left, immunoblotting for ZO-1 in triplicates of control DC2 cells (siRNAnc) and after CFTR knockdown (siRNAcftr). The same membrane was re-blotted for CFTR (middle panel) and for actin (lower panel). Right, quantification of ZO-1 expression normalized to actin. (C) qPCR analysis of ZO-1 mRNA (normalized to GAPDH) in controls (siRNAnc) and after CFTR knockdown (siRNAcftr). (D) Immunoblotting for ZO-1 in duplicates of control cells (siRNAnc) or siRNAcftr-treated cells that were treated with either vehicle (DMSO), the proteasome inhibitor MG-132 or the lysosome inhibitor leupeptin for 6 hours (left, upper panel). The same membranes were re-blotted for actin (left, lower panel). Quantification of ZO-1 normalized to actin (right). (E) Immunoblotting for CFTR and ZO-1 in DC2 cells after co-transfection with either siRNAnc or siRNAcftr and plasmid encoding human ZO-1 (pZO-1) or an empty vector (pVector). (F) TER measured after the Ca^{2+} switch experiment in DC2 cells under control conditions (siRNAnc) and after CFTR knockdown (siRNAcftr), in the absence (pVector) and presence of human ZO-1 overexpression (pZO1). Quantitative data show the mean±s.e.m.; *$P<0.05$; **$P<0.01$; ***$P<0.001$; ns, non-significant (two-way ANOVA).

of tight junctions in these cells. Cells transfected with siRNAcftr and pVector showed lower TER recovery after Ca^{2+} re-addition compared with that of control cells transfected with siRNAnc and pVector (Fig. 3F). By contrast, no significant difference in TER recovery was seen between cells transfected with siRNAcftr and siRNAnc when they were co-transfected with pZO-1.

CFTR controls the ZO-1–ZONAB pathway

We next examined the potential role of CFTR in the regulation of the ZO-1–ZONAB signaling pathway. The expression and localization of ZONAB was first assessed by immunofluorescence. As previously described in other cell types (Balda and Matter, 2000), confocal microscopy showed that ZONAB (green) was detected at tight junctions, identified by their immunoreactivity for ZO-1 (red), in confluent DC2 cells (Fig. 4A; siRNAnc). Cytoplasmic and weak nuclear ZONAB labeling were also detected. CFTR knockdown decreased the expression of ZONAB at tight junctions, but increased its nuclear localization (Fig. 4A; siRNAcftr). As described above, the ZO-1 labeling at tight junctions was more fragmented after CFTR knockdown compared with that of controls.

Journal of Cell Science (2014) 127, 4396–4408 doi:10.1242/jcs.148098

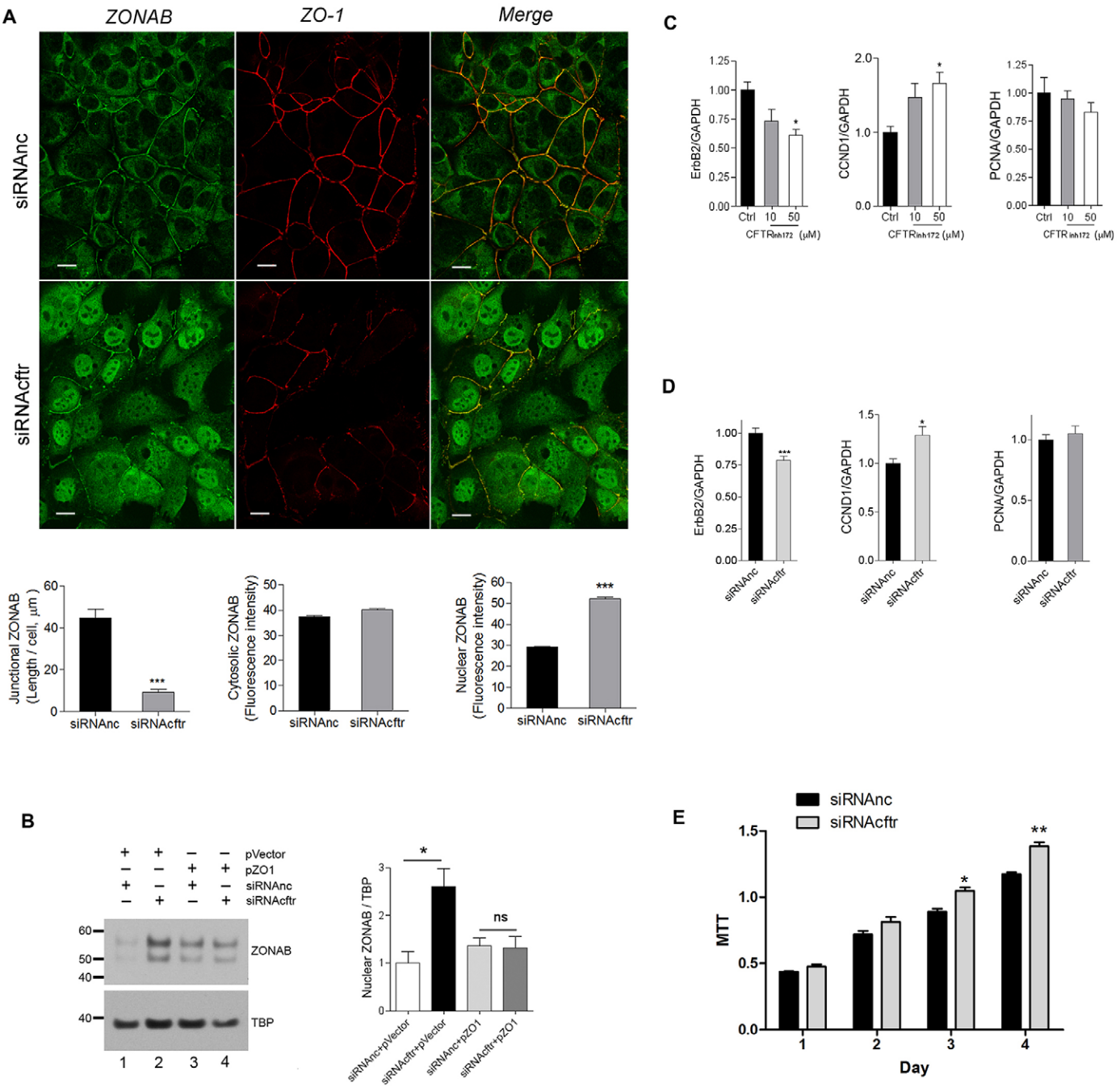

Fig. 4. CFTR controls the ZO-1–ZONAB pathway. (A) Double-immunofluorescence labeling for ZONAB (green) and ZO-1 (red) in control DC2 cells (siRNAnc) and after CFTR knockdown (siRNAcftr). Scale bar: 10 µm. Left bar graph, quantification of linear ZONAB located at tight junctions; middle bar graph, quantification of cytosolic ZONAB fluorescence intensity; right bar graph, quantification of nuclear ZONAB fluorescence intensity. (B) Left, immunoblotting for ZONAB in nuclear extracts from DC2 cells transfected as described for Fig. 3E. The same membrane was re-blotted for TBP. Right, quantification of nuclear ZONAB normalized for TBP. (C) qPCR analysis of ErbB2, CCND1 and PCNA mRNA expression in DC2 cells under control (Ctrl) conditions and in the presence of CFTRinh172 (10 and 50 µM). Data are normalized to controls and GAPDH was used as control (n=6). (D) qPCR analysis of ErbB2, CCND1 and PCNA mRNA expression in DC2 control cells (siRNAnc) and after CFTR knockdown (siRNAcftr). Data are normalized to controls and GAPDH was used as control (n=9). (E) Proliferation activity of DC2 control cells (siRNAnc) and after CFTR knockdown (siRNAcftr), determined using the MTT assay. Quantitative data show the mean±s.e.m.; *P<0.05; **P<0.01; ***P<0.001; ns, non-significant versus control (C) or siRNAnc (A,D,E); unpaired Student's t-test (A,D), one-way ANOVA (B,C), two-way ANOVA followed by Bonferroni's post hoc test (E).

Quantification of the linear tight junction labeling pattern (Fig. 4A, left bar graph) and mean fluorescence of the nuclear labeling (Fig. 4A, right bar graph), confirmed the translocation of ZONAB from tight junctions to the nucleus after CFTR knockdown. No effect was detected on the labeling intensity of cytosolic ZONAB (Fig. 4A, middle bar graph). The nuclear translocation of ZONAB induced following CFTR knockdown was confirmed by western blot analysis (Fig. 4B; compare lanes 1 and 2, siRNAcftr+pVector versus siRNAnc+pVector). Overexpression of ZO-1 with the pZO-1 vector prevented the nuclear translocation of ZONAB caused by

Journal of Cell Science (2014) 127, 4396–4408 doi:10.1242/jcs.148098

CFTR knockdown (Fig. 4B; compare lanes 3 and 4, siRNAcftr+pZO-1 versus siRNAnc+pZO-1). These results indicate that CFTR controls the subcellular localization of ZONAB by modulation of ZO-1 protein levels.

Previous studies showed that ZONAB, once located to the nucleus, promotes the transcription of cyclin D1 (CCND1) and proliferating cell nuclear antigen (PCNA), which are related to cell growth and proliferation (Sourisseau et al., 2006), and represses the transcription of ErbB2, a tyrosine kinase co-receptor important for epithelial differentiation and morphogenesis (Balda and Matter, 2000). We therefore examined the expression of these ZONAB-targeted genes by quantitative PCR. Both treatment with CFTRinh172 (10 and 50 µM, Fig. 4C) and CFTR knockdown (Fig. 4D) decreased the expression of ErbB2 but increased the amount of CCND1 mRNA in DC2 cells, although no significant difference in PCNA mRNA expression was found. These results demonstrate that CFTR regulates the expression of selected genes downstream of ZONAB. Moreover, DC2 cells transfected with siRNAcftr showed higher proliferation rates on day 3 and 4 after transfection, compared with siRNAnc controls (Fig. 4E).

CFTR expression precedes ZO-1 expression in tight junctions in the Wolffian duct

Immunofluorescence labeling of the mouse Wolffian duct on embryonic day 13.5 (E13.5) showed CFTR expression in the proximal, middle and distal portions of the duct (Fig. 5A). Higher magnification confocal microscopy pictures of Wolffian ducts double-labeled for CFTR and ZO-1 showed colocalization of CFTR and ZO-1 in epithelial tight junctions in the proximal portion of the duct (Fig. 5B). Interestingly, in the middle and distal portions of the Wolffian duct, ZO-1 was virtually undetectable, suggesting a less-developed state of the distal region compared with the proximal region at E13.5 (Fig. 5B, red). However, significant CFTR labeling was detected in all regions of the Wolffian duct at this time-point (Fig. 5B, green), suggesting that CFTR expression precedes that of ZO-1 during embryonic development.

The epididymis of CFTR-deficient mice shows alteration of ZO-1 and ZONAB expression and reduced epithelial differentiation

We then examined the regulation of ZO-1 and ZONAB by CFTR *in vivo*, using CFTR-knockout ($cftr^{-/-}$) mice. Immunofluorescent labeling showed reduced expression of ZO-1 in all regions of the epididymis, including the initial segment and cauda in $cftr^{-/-}$ mice compared with wild-type mice ($cftr^{+/+}$) (Fig. 6A). Quantification of the mean fluorescence intensity of ZO-1 labeling in tight junctions showed downregulation of ZO-1 in the initial segment, caput, corpus and cauda (Fig. 6B). ZO-1 expression was also assessed by western blotting in mice harboring the most frequent CF-associated mutation, ΔF508. A marked reduction of ZO-1 expression was observed in the epididymis of homozygous ΔF508 mice compared with their wild-type littermates (Fig. 6C). In addition, cell fractionation studies showed higher nuclear expression of ZONAB in the epididymis of ΔF508 mice compared with that of wild-type mice (Fig. 6D).

Histological analysis revealed that the epididymis of adult $cftr^{-/-}$ mice presents several alterations indicative of developmental defects and reduced epithelial differentiation. First, the overall size of the initial segment, caput and cauda was reduced in $cftr^{-/-}$ mice compared with that of $cftr^{+/+}$ mice

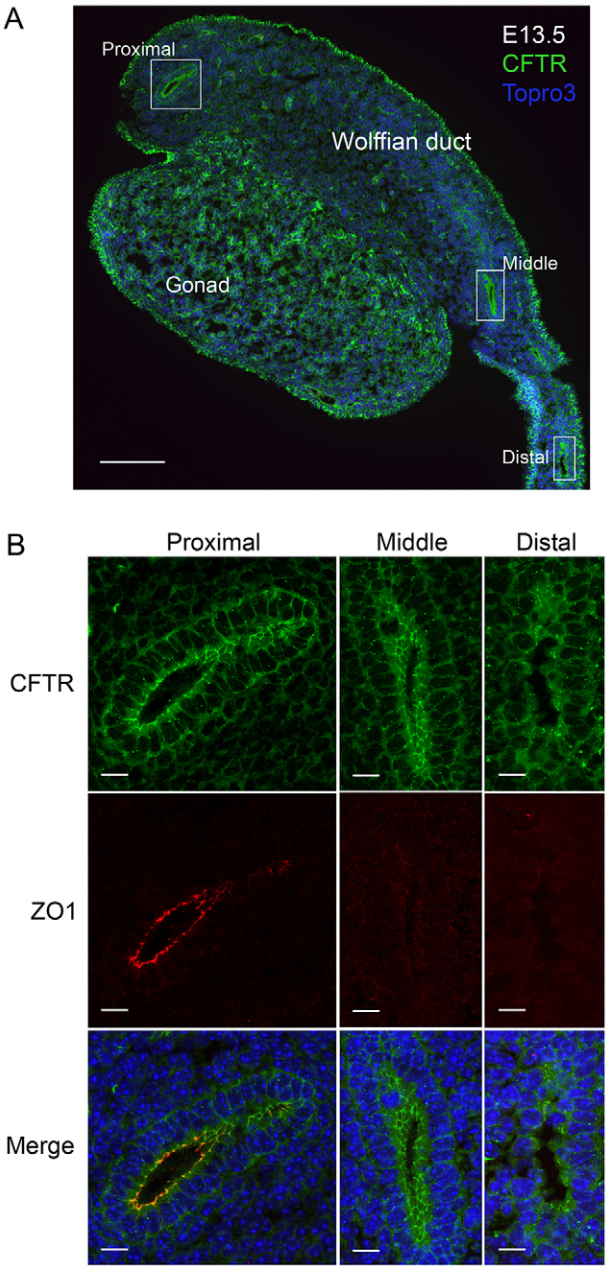

Fig. 5. CFTR and ZO-1 colocalization in the Wolffian duct. (A) CFTR immunofluorescence labeling (green) in mouse Wolffian duct and gonad at E13.5. Nuclei are labeled in blue with Topro-3. (B) Double-labeling for CFTR (green) and ZO-1 (red) in the proximal, middle and distal regions of the Wolffian duct delineated by the boxes in A. Scale bars: 100 µm (A); 10 µm (B).

(Fig. 6E). Accordingly, the weight of the epididymides was lower (Fig. 6F), and the diameter of tubules was significantly smaller in the initial segment, corpus and cauda regions in $cftr^{-/-}$ animals compared with that of $cftr^{+/+}$ mice (Fig. 6G). In addition, the height of the epithelium was lower in the initial segment and corpus, whereas it was higher in the cauda in $cftr^{-/-}$ mice compared with that of $cftr^{+/+}$ mice (Fig. 6H). Both these parameters indicate that deletion of CFTR causes a less-mature phenotype in the epididymis. This was confirmed by the lower expression of two independent markers of epithelial cell differentiation – the water and neutral solute channel aquaporin

Journal of Cell Science (2014) 127, 4396–4408 doi:10.1242/jcs.148098

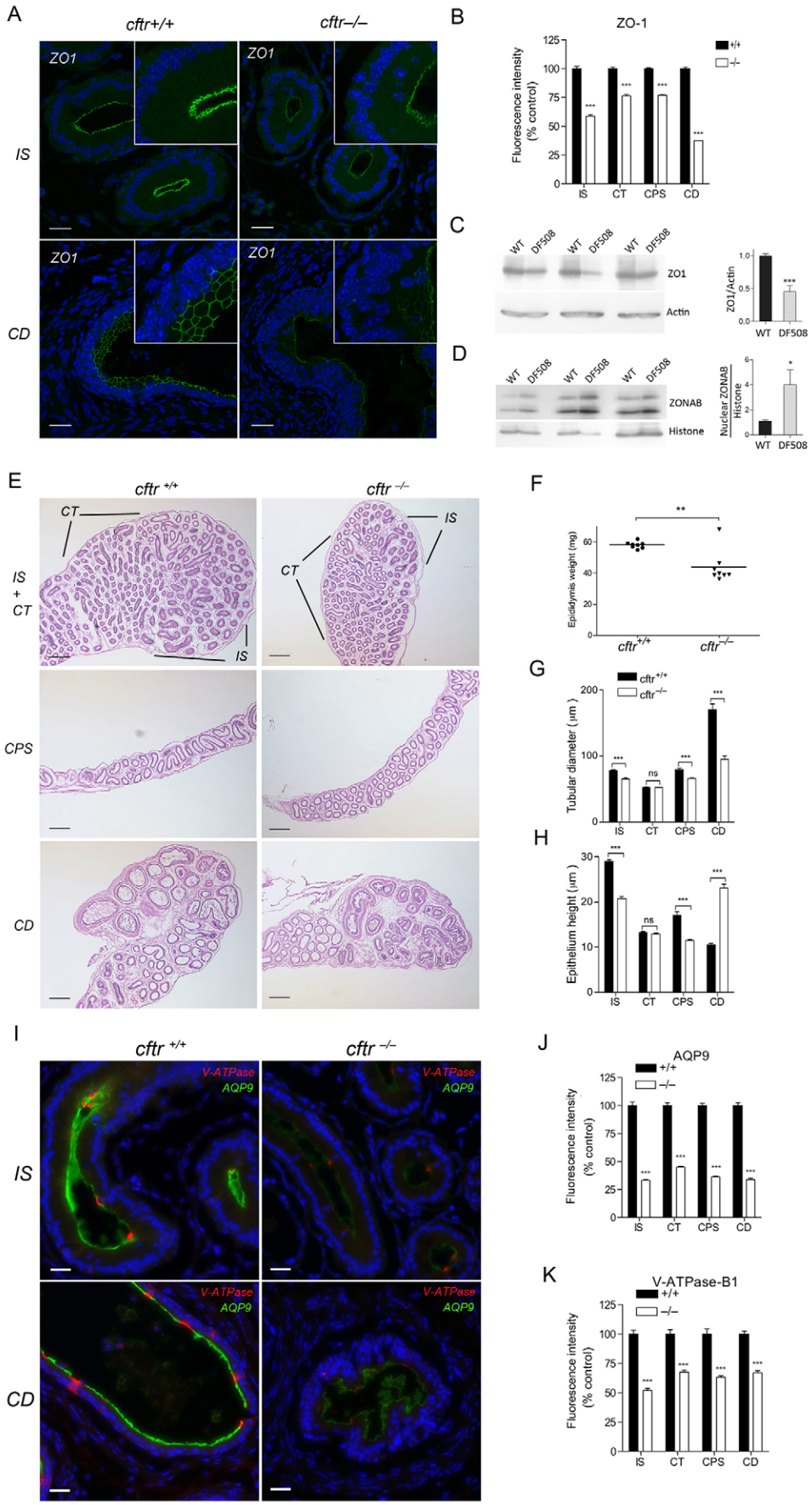

Fig. 6. Alteration of ZO-1 and ZONAB expression and developmental defects in CFTR-deficient mice.
(A) Immunofluorescent labeling for ZO-1 (green) in the initial segments (IS) and cauda (CD) regions of the epididymis from $cftr^{+/+}$ and $cftr^{-/-}$ mice. Nuclei are labeled in blue with DAPI. Scale bars: 20 μm. (B) Quantification of ZO-1 immunofluorescence showing a reduction in all regions of the epididymis in $cftr^{-/-}$ mice compared with $cftr^{+/+}$ mice. CT, caput; CPS, corpus. Initial segment, n=20; caput, n=273; corpus, n=417; cauda, n=96 tubule segments. (C) Immunoblotting for ZO-1 in the epididymis of $cftr^{1F508}$ mice (DF508) and their wild-type (WT) littermates. The same membrane was re-blotted for actin. (D) ZONAB immunoblots of nuclear epididymal extracts from DF508 controls and their wild-type littermates. The membrane was re-blotted for histone. (E) H&E staining of epididymis sections from $cftr^{+/+}$ and $cftr^{-/-}$ mice including the initial segment and caput, the corpus and the cauda regions. Scale bars: 250 μm. (F) The weight of epididymides in $cftr^{+/+}$ mice and $cftr^{-/-}$ mice. Horizontal lines show the means. (G) Tubular diameter in the initial segment, caput, corpus and cauda of $cftr^{-/-}$ mice and $cftr^{+/+}$ mice. (H) Epithelium height in the initial segment, caput, corpus and cauda of $cftr^{+/+}$ and $cftr^{-/-}$ mice. (I) Double-immunofluorescence labeling of epididymis sections for AQP9 (green) and V-ATPase-B1 (red) in the initial segment and cauda of $cftr^{+/+}$ and $cftr^{-/-}$ mice. Scale bars: 20 μm. Mean pixel intensity of AQP9 (J) and V-ATPase (K) immunofluorescence labeling in $cftr^{+/+}$ and $cftr^{-/-}$ mice. Quantitative data show the mean±s.e.m.; *P<0.05; **P<0.01; ***P<0.001; ns, non-significant [unpaired Student's t-test (C,D,F), two-way ANOVA (B,G,H,J,K)]

Journal of Cell Science (2014) 127, 4396–4408 doi:10.1242/jcs.148098

9 (AQP9) in principal cells (Pastor-Soler et al., 2001) and the proton-pump V-ATPase in clear cells (Brown et al., 1997; Pietrement et al., 2006) – in the epididymis of *cftr*$^{-/-}$ mice versus *cftr*$^{+/+}$ mice (Fig. 6I–K). Taken together, these results suggest impairment of epididymal development and differentiation in CFTR-deficient mice.

CFTR colocalizes with ZO-1 at the tight junctions of the trachea

Given the defects in tracheal development previously reported in human CF patients, we reassessed the localization of CFTR in this tissue. Double-labeling confocal microscopy for CFTR and ZO-1 revealed that, similar to the epididymis, CFTR is also located at ZO-1-positive tight junctions in the tracheal epithelium (Fig. 7; arrows).

DISCUSSION

The present study provides evidence that CFTR interacts with ZO-1 at tight junctions through its PDZ-binding domain, and controls gene expression by modulation of the ZO-1–ZONAB signaling pathway. We show here that CFTR, through its interaction with ZO-1, participates in the retention and/or recruitment of ZONAB at tight junctions, and that CFTR inhibition or knockdown induces the translocation of ZONAB into the nucleus, leading to upregulation of the proliferation-associated gene encoding CCND1 and downregulation of the differentiation-associated gene encoding ErbB2. We also observed an increased proliferative activity following CFTR knockdown. During development, as tubules elongate and tight junctions form, the subcellular localization of ZONAB determines when epithelial cells switch from a proliferative (nuclear ZONAB) to a differentiated (ZO-1-bound ZONAB at tight junctions) state (Balda and Matter, 2000; Balda and Matter, 2009; Lima et al., 2010; Sourisseau et al., 2006). Our data now identify CFTR as a central element for the regulation of epithelial cell plasticity during development, and provide a new paradigm for the etiology of pathologies associated with CFTR mutations, including CF.

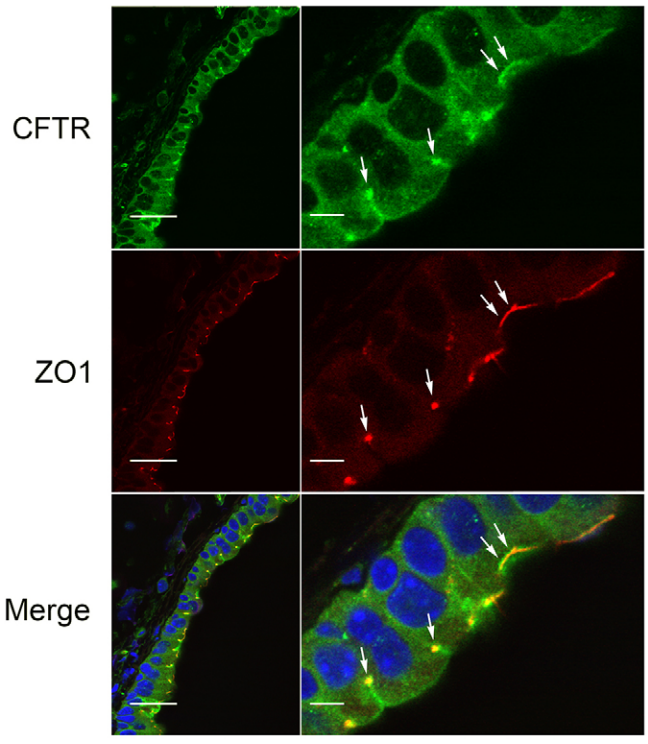

Fig. 7. CFTR and ZO-1 colocalization in the trachea. Laser scanning confocal imaging of mouse trachea double-labeled for CFTR (green) and ZO-1 (red), showing localization of CFTR at tight junctions. A weaker labeling for CFTR was also detected in the apical membrane. Arrows, colocalization of CFTR and ZO-1 at tight junctions. Scale bars: 20 µm (left); 5 µm (right).

Although a defect in the anion channel property of CFTR was originally considered to be the primary cause of CF, subsequent studies have shown that CFTR has the ability to interact with and regulate several other proteins, including other ion channels and transporters (Berdiev et al., 2009; Guggino and Stanton, 2006; Pietrement et al., 2008; Ruan et al., 2012; Yoo et al., 2004). Our results now add ZO-1 to the list of CFTR-interacting proteins and show that CFTR regulates the *de novo* formation of tight junctions as well as the reassembly of tight junctions following their disruption in a Ca^{2+} switch assay. We found that both murine CFTR (mouse epididymis and DC2 cells) and human CFTR (expressed in CHO cells) interact with ZO-1, demonstrating that the CFTR–ZO-1 interaction occurs across species. The PDZ-binding domain of CFTR mediates its interaction with other proteins (Guggino and Stanton, 2006), and we show here that it is also essential for the interaction of CFTR with ZO-1. Although ZO-1 contains three PDZ domains and could, therefore, bind directly to CFTR, further investigation is required to determine whether the CFTR–ZO-1 interaction is direct or occurs through interaction with other partners. This novel CFTR–ZO-1 interaction, together with the localization of CFTR at tight junctions of the Wolffian duct, indicates the participation of CFTR during embryonic development and tubulogenesis. This notion is supported by the absence of tubular structures in a 3D epididymal cell culture model after CFTR inhibition or knockdown. Interestingly, this effect was observed in the absence of cAMP stimulation, a condition that keeps the probability that the CFTR channel is open near zero. Thus the channel activity of CFTR does not appear to be required for its role in tight junction assembly. Indeed, we showed that CFTRinh172 reduced the amount of CFTR that co-immunoprecipitated with ZO-1 (supplementary material Fig. S1), indicating that the effects induced by this inhibitor on tight junction dynamics and tubulogenesis are mediated, at least partially, through impairment of the CFTR–ZO-1 interaction. Interestingly, a mutation at the CFTR C-terminus (where the PDZ-binding domain is located) has been reported in a CBAVD patient (Ostedgaard et al., 2003), illustrating the importance of this domain, and possibly of the CFTR–ZO-1 interaction, during development.

In previous studies, no obstruction was detected in the epididymis and vas deferens of human CF fetuses (Gaillard et al., 1997; Marcorelles et al., 2012). In addition, the epididymal abnormalities observed in infants and pre-pubertal boys with CF were reported to be less common than in adult CF patients (Blau et al., 2002; Gaillard et al., 1997; Oppenheimer and Esterly, 1969). Therefore, epididymal and vas deferens dysfunction in patients with CF might be the result of a progressive atrophy of these tissues that might occur relatively late during development and reach maximum intensity in adulthood. Interestingly, although the epididymides of human CF fetuses were reported to have a normal morphological appearance by microscopy during the first 22 weeks of gestation, a breakdown of the epithelial wall, accompanied by infiltration of inflammatory cells,

was detected in a human CF fetus at 26 weeks of gestation (Marcorelles et al., 2012). These focal areas of destruction were detected at a time when epithelial differentiation and apical accumulation of CFTR occur. These results are in agreement with our proposal that CFTR is an important modulator of epithelial cell differentiation. This is supported by our finding that the epididymis of adult *cftr*$^{-/-}$ mice has several features typical of an immature organ, including; (1) smaller organ weight, (2) reduction in tubule diameter, (3) increase in epithelial cell height in the cauda region and decrease in epithelial cell height in the initial segment, and (4) reduction in the expression of markers of epithelial cell differentiation (AQP9 in principal cells and V-ATPase in clear cells). Although *cftr*$^{-/-}$ male mice were initially reported to be fertile (O'Neal et al., 1993; Snouwaert et al., 1992), subsequent studies have shown that the vas deferens in *cftr*$^{-/-}$ mice have morphological abnormalities (Reynaert et al., 2000), and sperm from these mice have a lower fertilizing ability (Xu et al., 2007) (reviewed in Wilke et al., 2011). The epididymal abnormalities reported here further illustrate that CFTR depletion in mice induces an impaired male fertility phenotype. We also observed a more fragmented ZO-1 labeling in the epididymal tight junctions of *cftr*$^{-/-}$ mice compared with that of wild-type mice, indicating the role of CFTR in tight junction formation *in vivo*. In another mouse model harboring the most common CF-associated mutation, ΔF508, we found a reduction in total epididymal ZO-1 expression, together with an increased level of ZONAB in nuclear extracts. These results further support the notion that impairment of the ZO-1–ZONAB pathway secondary to CFTR mutations might affect the balance between proliferation and differentiation during development, leading to a progressive deterioration of tubule integrity and function.

In addition to the male reproductive tract, developmental defects were recently reported in the trachea of young CF patients and newborn CFTR-knockout pigs (Meyerholz et al., 2010). A previous report showed delayed differentiation and regeneration in non-infected human CF nasal epithelia (Hajj et al., 2007). In the present study, the lower TER that we observed after CFTR inhibition or knockdown in epididymal cells is in agreement with the modulation of paracellular permeability by CFTR previously reported in cultured airway epithelial cells (Castellani et al., 2012; LeSimple et al., 2010; Nilsson et al., 2010; Weiser et al., 2011). In these studies, several mechanisms were proposed to mediate the regulation of the paracellular pathway by apical membrane-bound CFTR, including the participation of NHERF1, ezrin, the RhoA–ROCK pathway, myosin II and tyrosine kinase phosphorylation. Our observation that CFTR is present in tracheal tight junctions sheds new light on the regulation of tight junctions by CFTR, and future studies will be required to determine whether these regulatory processes are involved in the CFTR-dependent modulation of the ZO-1–ZONAB pathway in the respiratory tract. Interestingly, a potential link between CFTR and epithelial cell polarization has previously been proposed (Hollande et al., 1998) but the underlying mechanism remained unclear. In addition, increased proliferative activity was observed in intestinal crypt epithelial cells of CFTR-null mice (Gallagher and Gottlieb, 2001). The present work, together with these previous studies, indicates the possible role of CFTR in the control of proliferation and differentiation through modulation of the ZONAB pathway in several tissues.

In conclusion, we propose that CFTR mutations cause impairment of epithelial development and repair secondary to deregulation of the ZO-1–ZONAB pathway. This leads to the downregulation of differentiation-associated genes and upregulation of proliferation-associated genes, and progressive weakening of tissues that become more susceptible to stress and injury. Other events that are caused by CFTR mutations, including reduced salt and water transport leading to a dehydrated luminal content (Guggino and Stanton, 2006), defective purinergic signaling (Ruan et al., 2012), bacterial colonization (Galietta, 2013) and reduced antimicrobial properties due to pH disturbances (Pezzulo et al., 2012) would all contribute to worsening the phenotype with progressive atrophy and dysfunction of several organs. Future strategies to treat CF should, therefore, address the role of CFTR in the establishment, remodeling and repair of epithelia.

MATERIALS AND METHODS

Antibodies

Antibodies used in the present study are listed in supplementary material Table S1 (primary antibodies) and Table S2 (secondary antibodies). The first part of our study was conducted using a commercial rabbit antibody against C-terminal amino acid residues 1468–1480 of human CFTR (Alomone Lab, ACL-006). We then produced an affinity-purified rabbit antibody against the same CFTR residues. Immunoblotting of mouse tissues using this antibody showed one band at ~160 kDa. The specificity of the antibody was also verified by peptide inhibition and siRNA-based knockdown assays.

Animals

Male C57BL/6 mice were purchased from Charles River Laboratories. All animal studies were approved by the Massachusetts General Hospital Subcommittee on Research Animal Care, in accordance with National Institutes of Health, Department of Agriculture and Accreditation of Laboratory Animal Care requirements. CFTR knockout mice (cftr$^{-/-}$) (Lu et al., 2012; Snouwaert et al., 1992) and cftr^{tm1Kth} mice harboring the ΔF508 CFTR mutation (Chen et al., 2012a; Zeiher et al., 1995) were maintained in a temperature-controlled room with a 12-hour light-dark cycle, with food and water *ad libitum*, in the Laboratory Animal Service Center at the Chinese University of Hong Kong. Littermates were used in comparison studies. All procedures were approved by the Animal Ethical Committee of the Chinese University of Hong Kong.

Tissue and cell fixation and cryo-sectioning

Adult wild-type male mice were anesthetized and perfused through the left ventricle with phosphate buffered saline (PBS) followed by a fixative buffer (PLP) containing 4% paraformaldehyde, 10 mM sodium periodate, 75 mM lysine and 5% sucrose in 0.1 M sodium phosphate buffer, as described previously (Ruan et al., 2012). Epididymides were dissected and further fixed by immersion in PLP for another 2 hours at room temperature. After three to five washes in PBS, tissues were stored in PBS containing 0.02% sodium azide at 4℃. Epididymides from cftr$^{-/-}$, cftr$^{+/+}$ and ΔF508 mice were fixed by immersion only in PLP for 4–5 hours at room temperature. Wild-type female and male mice were mated, and the presence of a vaginal plug the next morning was considered 0.5 days of gestation (E0.5). E13.5 gonads and Wolffian ducts were harvested and fixed by immersion in PLP. For cryosectioning, epididymides or E13.5 gonads or Wolffian ducts were cryoprotected in 30% sucrose in PBS containing 0.02% sodium azide at 4℃ for 24 hours, mounted in Tissue-Tek OCT compound 4583 (Sakura Fintek, Torrance, CA) and frozen at −20℃. Sections were cut to a thickness of 5–10 µm using a Leica CM3050-S cryomicrotome (Leica Microsystems, Buffalo, IL) and placed onto Superfrost/Plus microscope slides (Fisher Scientific, Pittsburg, PA). Cultured cells were fixed in PBS containing 4% paraformaldehyde for 20–30 minutes at room temperature.

Immunofluorescence

For epitope retrieval, sections were rehydrated in PBS for 5 minutes, heated in a microwave oven in an alkaline buffer (10 mM Tris buffer,

Journal of Cell Science (2014) 127, 4396–4408 doi:10.1242/jcs.148098

1 mM EDTA, pH 9.0) three to four times at 5-minute intervals, cooled down to room temperature and treated with 1% SDS in PBS for 4 minutes. For ZONAB labeling, DC2 cells were treated with 0.1% Triton X-100 for 10–15 minutes. For blocking, 1% bovine serum albumin (BSA) in PBS was applied for 15 minutes at room temperature. Sections were incubated with primary antibodies in a moist chamber for 90 minutes at room temperature or overnight at 4℃. They were washed in high-salt PBS [PBS containing 2.7% (w/v) NaCl] twice for 5 minutes and once in normal PBS. Fluorophore-conjugated secondary antibodies were applied for 1 hour, followed by washes as for the primary antibodies. Images were acquired with a Zeiss Radiance 2000 laser scanning confocal microscope (Zeiss Laboratories) using LaserSharp 2000 version 4.1 software. *Z*-series (1-µm intervals) were taken and imported into Volocity software (Improvision) for 3D reconstruction of cultured cells. Final animations were exported as Quicktime movies. Some images were also taken with a Nikon 80i epifluorescence microscope (Nikon Instruments, Melville, NY) using a Hamamatsu Orca charge-coupled device (CCD) camera (Hamamatsu, Bridgewater, NH) and IPLab scientific image processing software (Scanalytics Fairfax, VA). Images were imported into Adobe Photoshop software as TIFF files and the levels command was applied to the entire field of view to represent best the raw data visualized under the microscope.

Hematoxylin and Eosin staining

For Hematoxylin and Eosin (H&E) staining, sections were fixed in 95% ethanol for 1 minute, stained with Hematoxylin for 2 minutes and washed with tap water. They were then dipped into Bluing reagent a few times. Sections were then stained with Eosin for 5 seconds, dipped into 95% ethanol followed by 100% ethanol and xylene.

Image quantification

Perpendicularly cut tubules were selected from H&E-stained epididymis sections and the diameter of the entire tubule and epithelial height was measured using ImageJ software. To quantify the expression of ZO-1, AQP9 and V-ATPase, immunofluorescence images were acquired using identical parameters. Each image was corrected for its own luminal unstained background value, and the mean pixel intensity (MPI) of fluorescent labeling was measured using Volocity software. We have previously used this method to quantify expression of these markers in mouse and rat epididymis (Krapf et al., 2012; Pastor-Soler et al., 2002; Pastor-Soler et al., 2010). To quantify the level of ZONAB expression at tight junctions, the total length of linear ZONAB immunofluorescence labeling was quantified per cell in control DC2 cells (siRNAnc) and after CFTR knockdown (siRNAcftr). The level of nuclear ZONAB expression was quantified by measuring the MPI of ZONAB fluorescent labeling in the nuclei.

Cell culture

The immortalized epididymal cell line, DC2, was kindly provided by Marie-Claire Orgebin-Crist (Vanderbilt University School of Medicine, Nashville, TN), and cultured in Iscove's Modified Dulbecco's Medium (IMDM, Invitrogen) supplemented with 5α-di-hydrotestosterone (DHT, 1 nM) and 10% fetal bovine serum (FBS, Invitrogen) at 33℃ as previously described (Araki et al., 2002; Ruan et al., 2012). For 3D cultures, glass-bottomed culture chambers (356234, BD Biosciences) were coated with Matrigel (20 µl per well) on ice and placed in a 33℃ incubator for 20–30 minutes to stabilize the Matrigel. Suspended cells were then seeded onto the Matrigel layer at a density of 1×10^6 cells/ml and grown at 33℃. Chinese hamster ovary (CHO) cells were purchased from ATCC and cultured in F-12K medium (ATCC) supplemented with 10% FBS at 37℃.

Protein extraction

Tissues or cells were lysed for 30 minutes on ice in RIPA buffer (BostonBioproducts) containing complete protease inhibitors (Roche). Centrifugation was performed at 16,000 ***g*** for 30 minutes at 4℃, and the supernatant was collected. Protein concentration was determined using the bicinchoninic acid assay.

Immunoprecipitation

Protein extracts (250–1000 µg/reaction) were incubated with primary antibodies in an immunoprecipitation buffer containing 10 mM HEPES pH 7.5, 1001mM KCl, 2 mM $CaCl_2$, 2 mM $MgCl_2$ and complete protease inhibitors (Roche) (1 tablet for 4 ml buffer) overnight at 4℃. Magnetic beads conjugated to Protein A (Dynabeads®–Protein-A, Invitrogen) were washed with the immunoprecipitation buffer three times, and were then added to the protein–antibody complex (50 µl/reaction) and incubated for another 2–3 hours at 4℃. The protein–antibody–bead complexes were washed three times with the immunoprecipitation buffer using a magnetic separator. LDS Sample Buffer (Invitrogen) with 4% β-mercaptoethanol was added and shaken at 1400 rpm for 30 minutes at room temperature to denature the proteins and disassociate them from the beads.

Immunoblotting

Samples were prepared in LDS sample buffer (Invitrogen) with 4% β-mercaptoethanol and incubated for 30 minutes at room temperature. 30–100 µg protein was loaded into each well of 4–12% NuPAGE gels (Invitrogen) and separated by electrophoresis. After SDS-PAGE separation, proteins were transferred onto Immun-Blot polyvinylidene difluoride (PVDF) membranes (Bio-Rad). Membranes were blocked in Tris-buffered saline (TBS) containing 5% nonfat dry milk and then incubated overnight at 4℃ with the primary antibody diluted in TBS containing 2.5% milk. After three washes in TBS containing 0.1% Tween 20 (TBST), membranes were incubated with secondary antibody for 1 hour at room temperature. After three or four further washes, antibody binding was detected with the Western Lightning Chemiluminescence reagent (Perkin Elmer Life Sciences) and Kodak imaging films.

TER measurement

Cells were trypsinized and seeded onto permeable supports (0.4 µm, Costar) at a density of 1×10^5 cells/ml, and they were grown in the presence of CFTRinh172 or DMSO as controls. When siRNAs were applied, cells were plated at 2×10^5 cells/ml. The culture medium was changed immediately prior to TER measurement. The resistance was measured using Millicell Electrical Resistance System (Millipore) according to the manufacturer's instructions. Resistance across empty supports was measured each time as blank controls. TER values were determined by subtracting the value of blank controls from the total values. For the Ca^{2+} switch experiment, cells were grown for 3 days to achieve confluence. They were then incubated in a low-Ca^{2+} S-MEM medium (Invitrogen) supplemented with 5% dialyzed FBS (Invitrogen) for 3–4 hours. Cells were switched back to their regular growth medium, which contains normal levels of Ca^{2+}, and the TER was measured every hour for 3 hours.

MTT proliferation assay

Cells were plated at 2×10^5 cells/ml and an MTT kit (Sigma) was used to determine the proliferation rate of cells under control conditions and after CFTR knockdown.

siRNA-mediated interference

Stealth™ RNAi duplexes targeting mouse CFTR (5′-GAGAUUGAUG-GUGUCUCAUGGAAUU-3′, siRNAcftr), Low GC Stealth™ RNAi negative control duplexes (siRNAnc), Lipofectamine™ 2000 and Opti-MEM medium were purchased from Invitrogen. Lipofectamine 2000 and siRNAs were diluted with Opti-MEM. siRNA (100 nM) was transfected into DC2 cells with Lipofectamine 2000 using a reverse-transfection procedure, as described previously (Ruan et al., 2012).

RNA Extraction and reverse transcription

RNA was isolated using the RNeasy Mini Kit (Qiagen, Valencia, CA) and genomic DNA contamination was eliminated with the RNase-free DNase set (Qiagen). The isolated RNA was denatured at 70℃ in the presence of random hexamers (1.25 U/µl) and oligo dT (1.25 U/µl) for 10 minutes, and immediately transferred to ice. RNA was then converted into first-strand cDNA for 1 hour at 42℃ in 10 mM Tris-HCl pH 8.3,

50 mM KCl, 5 mM $MgCl_2$, 1 mM each dATP, dCTP, dGTP and dTTP, 1 U/µl RNase inhibitor and 2.5 U/µl murine leukemia virus reverse transcriptase (all reagents were from Applied Biosystems).

Quantitative polymerase chain reaction

Regular PCR was first performed and PCR products were resolved on an agarose gel as described previously (Ruan et al., 2012). The PCR product of each target gene was extracted from the gel using a gel extraction kit (Qiagen), diluted with water to achieve a series of concentrations and used as templates to generate standard curves for quantitative (q)PCR. qPCR was performed in 25 µl of reaction buffer, containing 5 µl of DNA template, 1×SYBR® Green Mixes (Applied Biosystems), 0.5 µM forward primer and 0.5 µM reverse primer. qPCR was performed in a 7300 Real-time PCR system (Applied Biosystems). The sequences of primers were as follows: mouse ErbB2, 5′-TAACTGGACCCCAGCCTATG-3′ and 5′-AACGGAGAATGACCCTGTTG-3′; mouse Ccnd1, 5′-GAGTCTCCGGTGCATCATTT-3′ and 5′-CAGCTTGCTAGGGAACTTGG-3′; mouse PCNA, 5′-CCACATTGGAGATGCTGTTG-3′ and 5′-CCGCCTCCTCTTCTTTATCC-3′; mouse Gapdh, 5′-GCACAGTCAAGGCCGAGAAT-3′ and 5′-GCCTTCTCCATGGTGGTGAA-3′; mouse ZO-1, 5′-GGGAGGGTCAAATGAAGACA-3′ and 5′-GGCATTCCTGCTGGTTACAT-3′.

Plasmid generation and transfection

The pCDNA3.1 plasmid expressing wild-type human CFTR (hCFTRwt) was generated as described previously (Zhou et al., 2005). The ΔDTRL-CFTR mutant, which lacks the C-terminal PDZ-binding domain (hCFTRΔpdzb), was generated by PCR-based mutagenesis (overlap extension PCR). PCR primers were as follows: primer 1, 5′-ACTGGCGGCCGC(*Not*I)TCTAGAACTAGTGGATC-3′; primer 2, 5′-GGAGACAGAAGAAGAGCTGCAATAGAGAGCAG-3′; primer 3, 5′-CAACATTTATGCTGCTCTCTTTGCACCTCT-3′; primer 4, 5′-GGGCCC(*Apa*I)CCCCTCGAGGTCGACGGTATCG-3′. These primers were synthesized by Tech Dragon (Hong Kong). All plasmids were verified by DNA sequence analysis performed by Tech Dragon (Hong Kong) or the DNA Core Facility at Massachusetts General Hospital. For transfection, CHO cells were grown until 60–70% confluence was achieved. DNA (3–7.5 µg per well for six-well plates) was transfected into CHO cells with Lipofectamine2000 (Invitrogen). Proteins were collected 48 hours after transfection. The pEGFP-ZO-1 was a gift from Alan Fanning (the University of North Carolina at Chapel Hill, NC; Addgene 30313).

Statistical analysis

Unpaired or paired Student's *t*-tests were applied to compare two groups. Multigroup comparisons were determined by one-way ANOVA followed by Bonferroni's post hoc tests. Multigroup comparisons involving more than one independent variable were determined by two-way ANOVA followed by Bonferroni's post hoc tests. Data show the mean±s.e.m. All tests were two-tailed, and statistical significance was set at $P<0.05$.

Competing interests

The authors declare no competing interests.

Author contributions

S.B., H.C.C., D.B. and Y.C.R. conceived of and designed the study; Y.C.R., R.Y.D., N.D.S., B.K., Y.W. and E.H. performed experiments; Y.C.R. and S.B. wrote the article with contributions from H.C.C. and D.B.

Funding

This work was supported by the National Institutes of Health [grant numbers HD040793 and DK097124 (to S.B.)]; and by the National 973 project [grant number 2012CV944903 to H.C.C.]. Y.C.R. was supported by a Lalor postdoctoral fellowship [grant number 2010–2012]. The Microscopy Core facility of the Massachusetts General Hospital (MGH) Program in Membrane Biology receives support from the Boston Area Diabetes and Endocrinology Research Center [grant number DK57521]; and the Center for the Study of Inflammatory Bowel Disease [grant number DK43341]. S.B. is a recipient of the Charles and Ann Sanders Research Scholar Award at MGH. Deposited in PMC for release after 12 months.

Supplementary material

Supplementary material available online at
http://jcs.biologists.org/lookup/suppl/doi:10.1242/jcs.148098/-/DC1

References

Anguiano, A., Oates, R. D., Amos, J. A., Dean, M., Gerrard, B., Stewart, C., Maher, T. A., White, M. B. and Milunsky, A. (1992). Congenital bilateral absence of the vas deferens. A primarily genital form of cystic fibrosis. *JAMA* **267**, 1794-1797.

Araki, Y., Suzuki, K., Matusik, R. J., Obinata, M. and Orgebin-Crist, M. C. (2002). Immortalized epididymal cell lines from transgenic mice overexpressing temperature-sensitive simian virus 40 large T-antigen gene. *J. Androl.* **23**, 854-869.

Balda, M. S. and Matter, K. (2000). The tight junction protein ZO-1 and an interacting transcription factor regulate ErbB-2 expression. *EMBO J.* **19**, 2024-2033.

Balda, M. S. and Matter, K. (2009). Tight junctions and the regulation of gene expression. *Biochim. Biophys. Acta* **1788**, 761-767.

Berdiev, B. K., Qadri, Y. J. and Benos, D. J. (2009). Assessment of the CFTR and ENaC association. *Mol. Biosyst.* **5**, 123-127.

Blau, H., Freud, E., Mussaffi, H., Werner, M., Konen, O. and Rathaus, V. (2002). Urogenital abnormalities in male children with cystic fibrosis. *Arch. Dis. Child.* **87**, 135-138.

Bomberger, J. M., Guggino, W. B. and Stanton, B. A. (2011). Methods to monitor cell surface expression and endocytic trafficking of CFTR in polarized epithelial cells. *Methods Mol. Biol.* **741**, 271-283.

Brown, D., Smith, P. J. and Breton, S. (1997). Role of V-ATPase-rich cells in acidification of the male reproductive tract. *J. Exp. Biol.* **200**, 257-262.

Castellani, S., Guerra, L., Favia, M., Di Gioia, S., Casavola, V. and Conese, M. (2012). NHERF1 and CFTR restore tight junction organisation and function in cystic fibrosis airway epithelial cells: role of ezrin and the RhoA/ROCK pathway. *Lab. Invest.* **92**, 1527-1540.

Chan, H. C., Ruan, Y. C., He, Q., Chen, M. H., Chen, H., Xu, W. M., Chen, W. Y., Xie, C., Zhang, X. H. and Zhou, Z. (2009). The cystic fibrosis transmembrane conductance regulator in reproductive health and disease. *J. Physiol.* **587**, 2187-2195.

Chen, H., Guo, J. H., Lu, Y. C., Ding, G. L., Yu, M. K., Tsang, L. L., Fok, K. L., Liu, X. M., Zhang, X. H., Chung, Y. W. et al. (2012a). Impaired CFTR-dependent amplification of FSH-stimulated estrogen production in cystic fibrosis and PCOS. *J. Clin. Endocrinol. Metab.* **97**, 923-932.

Chen, H., Ruan, Y. C., Xu, W. M., Chen, J. and Chan, H. C. (2012b). Regulation of male fertility by CFTR and implications in male infertility. *Hum. Reprod. Update* **18**, 703-713.

Cornwall, G. A. (2009). New insights into epididymal biology and function. *Hum. Reprod. Update* **15**, 213-227.

Cuppens, H. and Cassiman, J. J. (2004). CFTR mutations and polymorphisms in male infertility. *Int. J. Androl.* **27**, 251-256.

Fanning, A. S., Ma, T. Y. and Anderson, J. M. (2002). Isolation and functional characterization of the actin binding region in the tight junction protein ZO-1. *FASEB J.* **16**, 1835-1837.

Gaillard, D., Ruocco, S., Lallemand, A., Dalemans, W., Hinnrasky, J. and Puchelle, E. (1994). Immunohistochemical localization of cystic fibrosis transmembrane conductance regulator in human fetal airway and digestive mucosa. *Pediatr. Res.* **36**, 137-143.

Gaillard, D. A., Carré-Pigeon, F. and Lallemand, A. (1997). Normal vas deferens in fetuses with cystic fibrosis. *J. Urol.* **158**, 1549-1552.

Galietta, L. J. (2013). Managing the underlying cause of cystic fibrosis: a future role for potentiators and correctors. *Paediatr. Drugs* **15**, 393-402.

Gallagher, A. M. and Gottlieb, R. A. (2001). Proliferation, not apoptosis, alters epithelial cell migration in small intestine of CFTR null mice. *Am. J. Physiol.* **281**, G681-G687.

Guggino, W. B. and Stanton, B. A. (2006). New insights into cystic fibrosis: molecular switches that regulate CFTR. *Nat. Rev. Mol. Cell Biol.* **7**, 426-436.

Hajj, R., Lesimple, P., Nawrocki-Raby, B., Birembaut, P., Puchelle, E. and Coraux, C. (2007). Human airway surface epithelial regeneration is delayed and abnormal in cystic fibrosis. *J. Pathol.* **211**, 340-350.

Hihnala, S., Kujala, M., Toppari, J., Kere, J., Holmberg, C. and Höglund, P. (2006). Expression of SLC26A3, CFTR and NHE3 in the human male reproductive tract: role in male subfertility caused by congenital chloride diarrhoea. *Mol. Hum. Reprod.* **12**, 107-111.

Hollande, E., Fanjul, M., Chemin-Thomas, C., Devaux, C., Demolombe, S., Van Rietschoten, J., Guy-Crotte, O. and Figarella, C. (1998). Targeting of CFTR protein is linked to the polarization of human pancreatic duct cells in culture. *Eur. J. Cell Biol.* **76**, 220-227.

Joseph, A., Yao, H. and Hinton, B. T. (2009). Development and morphogenesis of the Wolffian/epididymal duct, more twists and turns. *Dev. Biol.* **325**, 6-14.

Katsuno, T., Umeda, K., Matsui, T., Hata, M., Tamura, A., Itoh, M., Takeuchi, K., Fujimori, T., Nabeshima, Y., Noda, T. et al. (2008). Deficiency of zonula occludens-1 causes embryonic lethal phenotype associated with defected yolk sac angiogenesis and apoptosis of embryonic cells. *Mol. Biol. Cell* **19**, 2465-2475.

Krapf, D., Ruan, Y. C., Wertheimer, E. V., Battistone, M. A., Pawlak, J. B., Sanjay, A., Pilder, S. H., Cuasnicu, P., Breton, S. and Visconti, P. E. (2012). cSrc is necessary for epididymal development and is incorporated into sperm during epididymal transit. *Dev. Biol.* **369**, 43-53.

LeSimple, P., Liao, J., Robert, R., Gruenert, D. C. and Hanrahan, J. W. (2010). Cystic fibrosis transmembrane conductance regulator trafficking modulates the barrier function of airway epithelial cell monolayers. *J. Physiol.* **588**, 1195-1209.
Li, X., Comellas, A. P., Karp, P. H., Ernst, S. E., Moninger, T. O., Gansemer, N. D., Taft, P. J., Pezzulo, A. A., Rector, M. V., Rossen, N. et al. (2012). CFTR is required for maximal transepithelial liquid transport in pig alveolar epithelia. *Am. J. Physiol.* **303**, L152-L160.
Lima, W. R., Parreira, K. S., Devuyst, O., Caplanusi, A., N'kuli, F., Marien, B., Van Der Smissen, P., Alves, P. M., Verroust, P., Christensen, E. I. et al. (2010). ZONAB promotes proliferation and represses differentiation of proximal tubule epithelial cells. *J. Am. Soc. Nephrol.* **21**, 478-488.
Lu, Y. C., Chen, H., Fok, K. L., Tsang, L. L., Yu, M. K., Zhang, X. H., Chen, J., Jiang, X., Chung, Y. W., Ma, A. C. et al. (2012). CFTR mediates bicarbonate-dependent activation of miR-125b in preimplantation embryo development. *Cell Res.* **22**, 1453-1466.
Ma, T., Thiagarajah, J. R., Yang, H., Sonawane, N. D., Folli, C., Galietta, L. J. and Verkman, A. S. (2002). Thiazolidinone CFTR inhibitor identified by high-throughput screening blocks cholera toxin-induced intestinal fluid secretion. *J. Clin. Invest.* **110**, 1651-1658.
Marcorelles, P., Gillet, D., Friocourt, G., Ledé, F., Samaison, L., Huguen, G. and Ferec, C. (2012). Cystic fibrosis transmembrane conductance regulator protein expression in the male excretory duct system during development. *Hum. Pathol.* **43**, 390-397.
Martinez-Palomo, A., Meza, I., Beaty, G. and Cereijido, M. (1980). Experimental modulation of occluding junctions in a cultured transporting epithelium. *J. Cell Biol.* **87**, 736-745.
Meyerholz, D. K., Stoltz, D. A., Namati, E., Ramachandran, S., Pezzulo, A. A., Smith, A. R., Rector, M. V., Suter, M. J., Kao, S., McLennan, G. et al. (2010). Loss of cystic fibrosis transmembrane conductance regulator function produces abnormalities in tracheal development in neonatal pigs and young children. *Am. J. Respir. Crit. Care Med.* **182**, 1251-1261.
Nilsson, H. E., Dragomir, A., Lazorova, L., Johannesson, M. and Roomans, G. M. (2010). CFTR and tight junctions in cultured bronchial epithelial cells. *Exp. Mol. Pathol.* **88**, 118-127.
O'Neal, W. K., Hasty, P., McCray, P. B., Jr, Casey, B., Rivera-Pérez, J., Welsh, M. J., Beaudet, A. L. and Bradley, A. (1993). A severe phenotype in mice with a duplication of exon 3 in the cystic fibrosis locus. *Hum. Mol. Genet.* **2**, 1561-1569.
O'Sullivan, B. P. and Freedman, S. D. (2009). Cystic fibrosis. *Lancet* **373**, 1891-1904.
Oates, R. D. and Amos, J. A. (1994). The genetic basis of congenital bilateral absence of the vas deferens and cystic fibrosis. *J. Androl.* **15**, 1-8.
Oppenheimer, E. H. and Esterly, J. R. (1969). Observations on cystic fibrosis of the pancreas. V. Developmental changes in the male genital system. *J. Pediatr.* **75**, 806-811.
Ostedgaard, L. S., Randak, C., Rokhlina, T., Karp, P., Vermeer, D., Ashbourne Excoffon, K. J. and Welsh, M. J. (2003). Effects of C-terminal deletions on cystic fibrosis transmembrane conductance regulator function in cystic fibrosis airway epithelia. *Proc. Natl. Acad. Sci. USA* **100**, 1937-1942.
Pastor-Soler, N., Bagnis, C., Sabolic, I., Tyszkowski, R., McKee, M., Van Hoek, A., Breton, S. and Brown, D. (2001). Aquaporin 9 expression along the male reproductive tract. *Biol. Reprod.* **65**, 384-393.
Pastor-Soler, N., Isnard-Bagnis, C., Herak-Kramberger, C., Sabolic, I., Van Hoek, A., Brown, D. and Breton, S. (2002). Expression of aquaporin 9 in the adult rat epididymal epithelium is modulated by androgens. *Biol. Reprod.* **66**, 1716-1722.
Pastor-Soler, N. M., Fisher, J. S., Sharpe, R., Hill, E., Van Hoek, A., Brown, D. and Breton, S. (2010). Aquaporin 9 expression in the developing rat epididymis is modulated by steroid hormones. *Reproduction* **139**, 613-621.
Patrizio, P. and Zielenski, J. (1996). Congenital absence of the vas deferens: a mild form of cystic fibrosis. *Mol. Med. Today* **2**, 24-31.
Pezzulo, A. A., Tang, X. X., Hoegger, M. J., Alaiwa, M. H., Ramachandran, S., Moninger, T. O., Karp, P. H., Wohlford-Lenane, C. L., Haagsman, H. P. et al. (2012). Reduced airway surface pH impairs bacterial killing in the porcine cystic fibrosis lung. *Nature* **487**, 109-113.
Pietrement, C., Sun-Wada, G. H., Silva, N. D., McKee, M., Marshansky, V., Brown, D., Futai, M. and Breton, S. (2006). Distinct expression patterns of different subunit isoforms of the V-ATPase in the rat epididymis. *Biol. Reprod.* **74**, 185-194.
Pietrement, C., Da Silva, N., Silberstein, C., James, M., Marsolais, M., Van Hoek, A., Brown, D., Pastor-Soler, N., Ameen, N., Laprade, R. et al. (2008). Role of NHERF1, cystic fibrosis transmembrane conductance regulator, and cAMP in the regulation of aquaporin 9. *J. Biol. Chem.* **283**, 2986-2996.
Quinton, P. M. (1999). Physiological basis of cystic fibrosis: a historical perspective. *Physiol. Rev.* **79 Suppl.**, S3-S22.
Ramsey, B. W., Banks-Schlegel, S., Accurso, F. J., Boucher, R. C., Cutting, G. R., Engelhardt, J. F., Guggino, W. B., Karp, C. L., Knowles, M. R., Kolls, J. K. et al. (2012). Future directions in early cystic fibrosis lung disease research: an NHLBI workshop report. *Am. J. Respir. Crit. Care Med.* **185**, 887-892.
Reynaert, I., Van Der Schueren, B., Degeest, G., Manin, M., Cuppens, H., Scholte, B. and Cassiman, J. J. (2000). Morphological changes in the vas deferens and expression of the cystic fibrosis transmembrane conductance regulator (CFTR) in control, deltaF508 and knock-out CFTR mice during postnatal life. *Mol. Reprod. Dev.* **55**, 125-135.
Robaire, B., Hinton, B. T. and Orgebin-Crist, M. C. (2006). The epididymis. In *Physiology of Reproduction* (ed. J. D. Neill), pp. 1071-1148. New York, NY: Elsevier.
Rowe, S. M. and Verkman, A. S. (2013). Cystic fibrosis transmembrane regulator correctors and potentiators. *Cold Spring Harb. Perspect Med.* **3**, a009761.
Rowe, S. M., Miller, S. and Sorscher, E. J. (2005). Cystic fibrosis. *N. Engl. J. Med.* **352**, 1992-2001.
Ruan, Y. C., Shum, W. W., Belleannée, C., Da Silva, N. and Breton, S. (2012). ATP secretion in the male reproductive tract: essential role of CFTR. *J. Physiol.* **590**, 4209-4222.
Ruz, R., Andonian, S. and Hermo, L. (2004). Immunolocalization and regulation of cystic fibrosis transmembrane conductance regulator in the adult rat epididymis. *J. Androl.* **25**, 265-273.
Schulz, S., Jakubiczka, S., Kropf, S., Nickel, I., Muschke, P. and Kleinstein, J. (2006). Increased frequency of cystic fibrosis transmembrane conductance regulator gene mutations in infertile males. *Fertil. Steril.* **85**, 135-138.
Shum, W. W., Ruan, Y. C., Da Silva, N. and Breton, S. (2011). Establishment of cell-cell cross talk in the epididymis: control of luminal acidification. *J. Androl.* **32**, 576-586.
Snouwaert, J. N., Brigman, K. K., Latour, A. M., Malouf, N. N., Boucher, R. C., Smithies, O. and Koller, B. H. (1992). An animal model for cystic fibrosis made by gene targeting. *Science* **257**, 1083-1088.
Sourisseau, T., Georgiadis, A., Tsapara, A., Ali, R. R., Pestell, R., Matter, K. and Balda, M. S. (2006). Regulation of PCNA and cyclin D1 expression and epithelial morphogenesis by the ZO-1-regulated transcription factor ZONAB/DbpA. *Mol. Cell. Biol.* **26**, 2387-2398.
Tizzano, E. F., Chitayat, D. and Buchwald, M. (1993). Cell-specific localization of CFTR mRNA shows developmentally regulated expression in human fetal tissues. *Hum. Mol. Genet.* **2**, 219-224.
van der Ven, K., Messer, L., van der Ven, H., Jeyendran, R. S. and Ober, C. (1996). Cystic fibrosis mutation screening in healthy men with reduced sperm quality. *Hum. Reprod.* **11**, 513-517.
Weiser, N., Molenda, N., Urbanova, K., Bähler, M., Pieper, U., Oberleithner, H. and Schillers, H. (2011). Paracellular permeability of bronchial epithelium is controlled by CFTR. *Cell. Physiol. Biochem.* **28**, 289-296.
Wilke, M., Buijs-Offerman, R. M., Aarbiou, J., Colledge, W. H., Sheppard, D. N., Touqui, L., Bot, A., Jorna, H., de Jonge, H. R. and Scholte, B. J. (2011). Mouse models of cystic fibrosis: phenotypic analysis and research applications. *J. Cyst. Fibros.* **10 Suppl. 2**, S152-S171.
Xu, W. M., Shi, Q. X., Chen, W. Y., Zhou, C. X., Ni, Y., Rowlands, D. K., Yi Liu, G., Zhu, H., Ma, Z. G., Wang, X. F. et al. (2007). Cystic fibrosis transmembrane conductance regulator is vital to sperm fertilizing capacity and male fertility. *Proc. Natl. Acad. Sci. USA* **104**, 9816-9821.
Yoo, D., Flagg, T. P., Olsen, O., Raghuram, V., Foskett, J. K. and Welling, P. A. (2004). Assembly and trafficking of a multiprotein ROMK (Kir 1.1) channel complex by PDZ interactions. *J. Biol. Chem.* **279**, 6863-6873.
Yu, J., Chen, Z., Ni, Y. and Li, Z. (2012). CFTR mutations in men with congenital bilateral absence of the vas deferens (CBAVD): a systemic review and meta-analysis. *Hum. Reprod.* **27**, 25-35.
Zeiher, B. G., Eichwald, E., Zabner, J., Smith, J. J., Puga, A. P., McCray, P. B., Jr, Capecchi, M. R., Welsh, M. J. and Thomas, K. R. (1995). A mouse model for the delta F508 allele of cystic fibrosis. *J. Clin. Invest.* **96**, 2051-2064.
Zhou, Z., Wang, X., Li, M., Sohma, Y., Zou, X. and Hwang, T. C. (2005). High affinity ATP/ADP analogues as new tools for studying CFTR gating. *J. Physiol.* **569**, 447-457.